

Article

# Cellular Uptake and Phototoxicity Optimization of Arene Ruthenium Porphyrin Derivatives

Zeinab Janbeih <sup>1</sup>, Manuel Gallardo-Villagrán <sup>2,3</sup>, Bruno Therrien <sup>3</sup> , Mona Diab-Assaf <sup>4</sup>, Bertrand Liagre <sup>2,\*</sup>   
and Ludmil Benov <sup>1</sup> 

<sup>1</sup> Biochemistry Department, Faculty of Medicine, Kuwait University, Kuwait City 12037, Kuwait; zeinab.janbeih@etu.unilim.fr (Z.J.); ludmil.benov@ku.edu.kw (L.B.)

<sup>2</sup> Univ. Limoges, LABCiS, UR 22722, Faculté de Pharmacie, F-87000 Limoges, France; villagran@outlook.com

<sup>3</sup> Institut de Chimie, Université de Neuchâtel, Avenue de Bellevaux 51, CH-2000 Neuchâtel, Switzerland; bruno.therrien@unine.ch

<sup>4</sup> Doctoral School of Sciences and Technology, Lebanese University, Hadath, Beirut 21219, Lebanon; mdiabassaf@ul.edu.lb

\* Correspondence: bertrand.liagre@unilim.fr

**Abstract:** In this study, dinuclear and tetranuclear arene ruthenium porphyrins were synthesized and assessed for their potential as photosensitizers (PSs) in photodynamic therapy (PDT) using the Colo205 colon cancer cell line as a model system. Reactive oxygen species (ROS) production, cellular uptake, impact on cell viability, and mechanisms of cell death induced by the synthesized compounds were comprehensively investigated. Our results revealed that the number of arene ruthenium units, as well as zinc (Zn) metalation of the porphyrin core, significantly influenced ROS production and increased it two-folds compared to the Zn-free analogs. The uptake of tetra-substituted Zn-porphyrins by the cancer cells increased to 2.8 nmol/10<sup>6</sup> cells compared to 0.6 nmol/10<sup>6</sup> cells of the disubstituted Zn-free and Zn-chelating porphyrins. The anticancer photo-activity of the complexes, where the percentage of metabolic activity of disubstituted Zn-porphyrins decreased to 26% when Zn was inserted, was compared to disubstituted Zn-free analogs. A further decrease in metabolic activity was observed, when the number of arene ruthenium units increased in the tetra-substituted Zn-porphyrins and tetra-substituted Zn-free compounds, reaching 4% and 14% respectively. Moreover, the percentage of apoptotic cell deaths increased to 40% when Zn was inserted into disubstituted porphyrins, compared to disubstituted Zn-free analog, and 50% when the number of arene ruthenium units increased. Overall, the tetra-substituted Zn chelating porphyrins exhibited the highest PDT efficiency, followed by the di-substituted Zn-porphyrins. These findings underscore the importance of structural design in optimizing the efficacy of arene ruthenium porphyrins as PSs for PDT, offering valuable insights for the development of targeted cancer therapeutics.

**Keywords:** photodynamic therapy; arene ruthenium complexes; porphyrin; colon cancer; photosensitizers



**Citation:** Janbeih, Z.; Gallardo-Villagrán, M.; Therrien, B.; Diab-Assaf, M.; Liagre, B.; Benov, L. Cellular Uptake and Phototoxicity Optimization of Arene Ruthenium Porphyrin Derivatives. *Inorganics* **2024**, *12*, 86. <https://doi.org/10.3390/inorganics12030086>

Academic Editor: Axel Klein

Received: 21 January 2024

Revised: 5 March 2024

Accepted: 6 March 2024

Published: 12 March 2024



**Copyright:** © 2024 by the authors. Licensee MDPI, Basel, Switzerland. This article is an open access article distributed under the terms and conditions of the Creative Commons Attribution (CC BY) license (<https://creativecommons.org/licenses/by/4.0/>).

## 1. Introduction

Colorectal cancer (CRC) is a leading cause of cancer-related death. Worldwide, there are over a million new cases of CRC being diagnosed each year. CRC is known to be the third most frequent malignancy and the fourth most frequent cause of cancer-related death [1]. Most CRCs are developed as a complex process involving multiple biomolecular pathways, from the formation of adenomas to the development of carcinomas in the digestive tract [2]. Chemotherapy, radiation therapy, targeted therapy, and surgery are common treatment modalities for CRC [3]. The choice of treatment is solely dependent on the stage of the disease.

Photodynamic therapy (PDT) using photosensitizers (PSs) like porphyrin or chlorin derivatives is receiving attention as a treatment for CRC [4]. The advantages of PDT make it attractive when compared to other cancer therapies, such as chemotherapy, radiation,

and surgery, and it can be applied in combination with other methods when needed [5]. By nature, PDT is selective, which allows for minimal toxicity when it comes to normal tissues surrounding the tumor. In fact, PDT has negligible systemic side effects since it is based on treating only the areas where the disease occurs. Additionally, PDT is repeatable, having no cumulative dose limitations as opposed to both chemotherapy and radiotherapy, and can replace conventional tumor ablative therapies [5]. Moreover, PDT can be used when surgery is not a possible option.

PDT is based on the administration of PSs followed by irradiation of the target area with light at an appropriate wavelength. Upon absorption of light, the PS becomes excited, and after reaching a triplet state, it can participate in two types of photochemical reactions, type 1 and type 2, respectively. In type 1, the excited PS participates in a redox reaction with neighboring molecules by transferring an electron to form a radical anion or a radical cation. Such radicals could further react with oxygen to produce reactive oxygen species (ROS). In type 2 processes, the excited PS in a triplet state transfers energy to molecular oxygen, resulting in the formation of singlet oxygen ( $^1\text{O}_2$ ) which can form adducts with organic substrates including DNA, RNA, proteins, and lipids [6,7]. Therefore, cellular structures and biomolecules could be damaged to an extent that leads to cell death.

Singlet oxygen is a powerful oxidant that can react with biomolecules. Singlet oxygen has a short lifetime (10–40 ns in the cytoplasm) and an estimated diffusion distance corresponding to 10–20 nm [8]. Therefore, damage of the subcellular structures occurs close to the site of the  $^1\text{O}_2$  formation [9]. Consequently, targeting specific subcellular structures seems to be a good strategy to enhance PDT efficacy [9]. The extent of PDT-induced damage and its nature determine the predominant mechanism of cell death [10]. The damaged site depends on the PS structure because different PSs accumulate in different cell compartments [11]. It has been shown that the overall charge, charge distribution, and lipophilicity of the PS are important parameters that control cellular uptake and subcellular distribution [12,13].

Insertion of zinc in porphyrins is expected to enhance PDT efficacy by increasing the triplet lifetimes of the PSs, which in turn increases the chances for collision with other molecules and energy transfer to oxygen, leading to the production of singlet oxygen or electron transfer resulting in the generation of radicals [14,15]. However, other studies contradict these findings and have shown that the presence of zinc worsens PDT efficacy on human melanoma and synovial sarcoma, where a metal-free derivative shows a higher activity than its zinc analogues [16,17]. Moreover, these studies worked on hydrophobic PSs with low solubility in water environments and biological media, which tend to aggregate and were not taken up by melanoma cells [16]. Therefore, there is a necessity to investigate the compound's behavior and its uptake by cells using different methods. Increasing the solubility of compounds without increasing the dose can be achieved by encapsulation of the PS in nanoparticles [18], by coordination to peptides [19], entrapment in lysosomes [20], or by adding hydrophilic substituents like phosphates or sulfonates [21]. The aim of the current study was to examine how zinc insertion and substitutions at the periphery of a tetrapyrrole ring affect the photodynamic activity and uptake of arene ruthenium porphyrin derivatives in Colo205 cells in the absence and presence of light.

Ruthenium organometallic compounds have been used for years and are not new to PDT. The reasons behind the choice of ruthenium (II) are its oxidation state stability and its almost non-reactivity to oxygen, air, and water, unlike other metal-based compounds [17,22], as well as its high coordination number, high facility to coordinate with ligands of complexed structures [22], ability to interact with DNA and proteins [23], and lower general toxicity compared to its platinum counterparts [18]. Accordingly, we have used eight complexes with either two or four arene ruthenium units (arene = *p*-cymene, or phenylpropanol) at the periphery of four porphyrin derivatives—5,10,15,20-tetra(4-pyridyl)porphyrin, 5,10,15,20-tetra(4-pyridyl)porphyrin-Zn, 5,15-di(4-pyridyl)-10,20-diphenylporphyrin, and 5,15-di(4-pyridyl)-10,20-diphenylporphyrin-Zn—in an attempt to combine the photodynamic activity of porphyrins with the cytotoxicity of ruthenium

complexes—and also because they have exhibited good phototoxic and cytotoxic properties against other cell lines, such as synovial sarcoma, prostate cancer, oral cancer, and human melanoma [16,17].

## 2. Results and Discussion

### 2.1. Spectral Properties

The structures of all di- and tetranuclear complexes (Figure 1) were confirmed by  $^1\text{H}$  NMR data, by comparison with the literature [16]. The absorption peaks and molar extinction coefficients of the arene ruthenium porphyrin derivatives are presented in Table S1. The arene ruthenium compounds exhibit three Q bands between 510 and 650 nm and an intense Soret-type band around 420 nm.

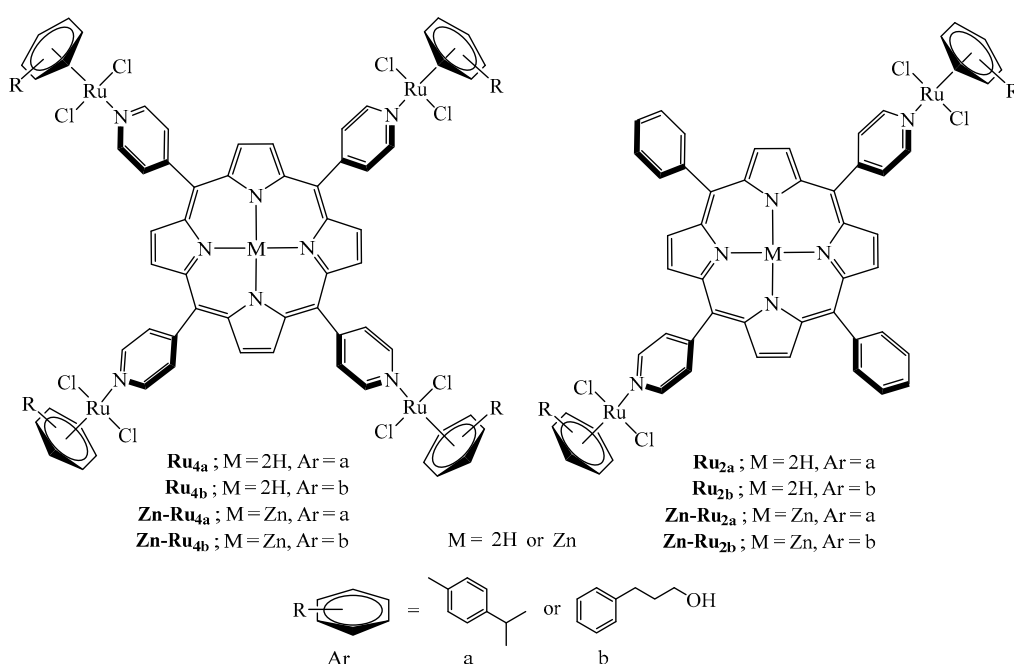


**Figure 1.** Structures of the arene ruthenium porphyrin derivatives used in this study.

### 2.2. Production of Reactive Oxygen Species

1,3-Diphenylisobenzofuran (DPBF), which reacts with  $^1\text{O}_2$ ,  $\text{H}_2\text{O}_2$ ,  $\text{HO}\cdot$ ,  $\text{RO}\cdot$ ,  $\text{ROO}\cdot$ , and reactive nitrogen species and can serve as an indicator of an oxidative cellular stress, was used to determine the efficacy of the tested RuPs in generating cell-damaging species [24].

The results shown in Figure 2 demonstrate that the Zn-containing derivatives were more efficient generators of ROS than the metal-free porphyrin derivatives. The highest amount of ROS production was observed for the tetra-substituted derivatives  $\text{Zn-Ru}_{4b}$  and  $\text{Zn-Ru}_{4a}$ , followed by the  $\text{Zn-Ru}_2$  derivatives ( $\text{Zn-Ru}_{2a}$  and  $\text{Zn-Ru}_{2b}$ ). The introduction of zinc increases the triplet lifetimes of the PSs, which in turn increases the chances for collision with other molecules and energy transfer to oxygen leading to the production of singlet oxygen or electron transfer, resulting in the generation of radicals [14,15]. Among the Zn-free derivatives, the tetra-substituted  $\text{Ru}_{4a}$  and  $\text{Ru}_{4b}$  were slightly more efficient generators of ROS than the di-substituted compounds  $\text{Ru}_{2a}$  and  $\text{Ru}_{2b}$ .

### 2.3. Effect of PDT on Metabolic Activity

An active metabolism is essential for cell proliferation, and targeting the metabolism of cancer cells is a promising strategy in anticancer therapy [25]. Depending on the extent of the photodamage, the properties of the PSs, and the nature of the cellular targets, PDT-treated cells can either repair the photodamage and recover after the treatment or die, if destructive reactions prevail [26,27]. It has been demonstrated that reactions initi-

ated during photodynamic treatment can continue after cessation of illumination, leading to suppression of metabolic activity and loss of viability [28]. In order to assess the delayed consequences of PDT treatment, cell metabolic activity was assessed 24 h after PDT treatment.

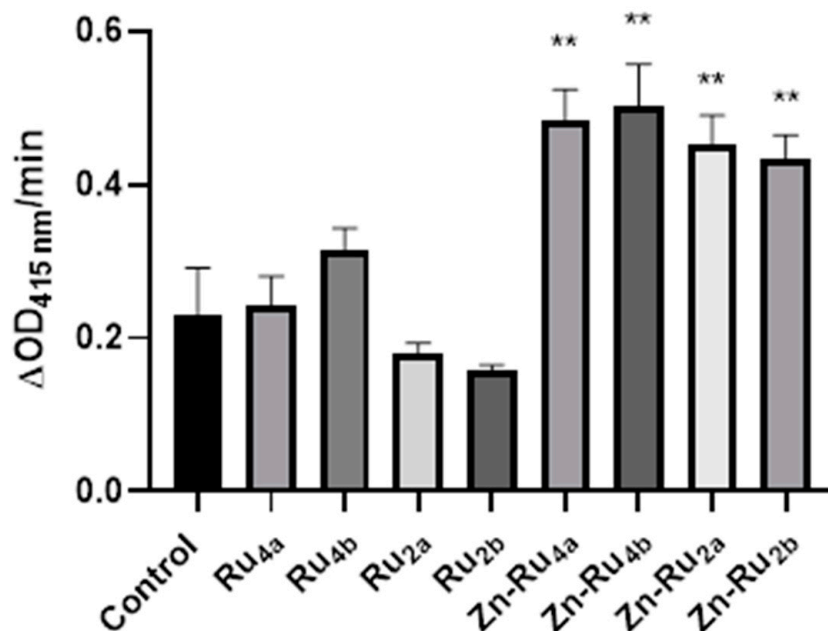


**Figure 2.** Production of ROS. Tested compounds (1  $\mu$ M) were added to 3 mL of a reaction mixture containing 50  $\mu$ M of 1,3-diphenylisobenzofuran (DPBF) in of 9:1 dimethylformamide (DMF): deionized water. The mixture was illuminated in a quartz cuvette at a fluence of 95 mW/cm<sup>2</sup>. Data are presented as mean  $\pm$  S.D. (n = 3). \*\* indicates  $p < 0.01$  compared to control.

The MTT assay is commonly used to determine cell viability. Since MTT reduction to colored formazan is enzymatic and depends on availability of NAD(P)H, it reflects cellular metabolic activity. In the current study, the MTT assay was used to obtain information about the effect of photodynamic treatment on the overall metabolic activity. Figure 3 shows that the efficacy of the tested PSs in suppressing cancer cell's metabolism parallels ROS production. The tetra-substituted Zn-chelated Ru-porphyrins, **Zn-Ru<sub>4b</sub>** and **Zn-Ru<sub>4a</sub>** were the most efficient in all tested concentrations, followed by the di-substituted **Zn-Ru<sub>2a</sub>** and **Zn-Ru<sub>2b</sub>**. Among the Zn-free derivatives, again, the tetra-substituted **Ru<sub>4b</sub>** and **Ru<sub>4a</sub>** demonstrated higher PDT activity than the corresponding di-substituted **Ru<sub>2a</sub>** and **Ru<sub>2b</sub>**. This effect was entirely light-dependent and, at concentrations of up to 5  $\mu$ M, none of the tested compounds showed dark toxicity, as shown in Figure S2.

#### 2.4. Cell Proliferation

Suppression of cell division is a major goal of anticancer treatment. Cell proliferation requires an adequate supply of ATP, reducing equivalents, acetyl-CoA, and amino acids [29], and it is conceivable that PSs which inhibit metabolic activity would be efficient in preventing cell multiplication. Indeed, the results presented in Figure 4 demonstrate that, at 5  $\mu$ M, all arene ruthenium complexes, except the di-substituted Zn-free derivatives **Ru<sub>2a</sub>** and **Ru<sub>2b</sub>**, completely suppressed cell division. No effect of the tested compounds on cell proliferation was observed in the absence of illumination, as shown in Figure S3.

Comparison of the data presented in Figures 2 and 4 shows that the tetra-substituted **Zn-Ru<sub>4</sub>** and **Ru<sub>4</sub>** derivatives differ with respect to ROS production but were equally efficient in blocking cell division. The di-substituted ruthenium porphyrins, **Ru<sub>2a</sub>** and **Ru<sub>2b</sub>**, which displayed the lowest yield of ROS production, did not show antiproliferative photodynamic activity.

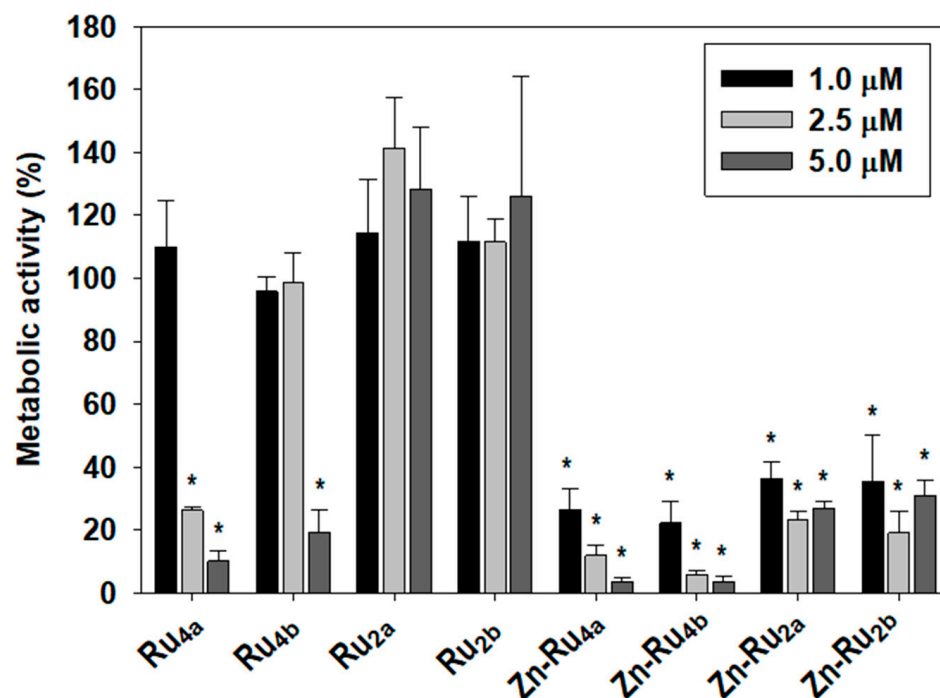


**Figure 3.** Effect of photodynamic treatment on metabolic activity. Cells were preincubated with 1, 2.5, and 5  $\mu\text{M}$  of PSs for 24 h in the dark and were illuminated for 30 min at a fluence of 95  $\text{mW}/\text{cm}^2$ . Metabolic activity was determined by the MTT assay and presented as a percentage of MTT reduction to formazan. Mean  $\pm$  S.D. of three independent experiments, each sample in triplicate is presented. \* indicates  $p < 0.05$  compared to control.

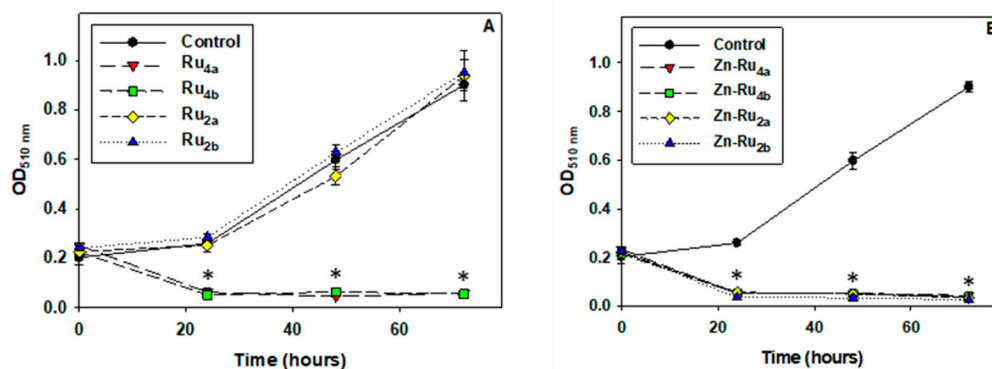


**Figure 4.** Effect of photo-treatment on cell proliferation. Cell cultures were preincubated with 5  $\mu\text{M}$  PSs for 24 h, illuminated for 30 min, and SRB assay was then performed. Results are presented as OD510 nm corresponding to the number of adhered viable cells. Zn-free Ru-porphyrins (A) and Zn-Ru derivatives (B). Data are expressed as mean  $\pm$  S.D. of three independent experiments. \* indicates  $p < 0.05$  compared to control.

High  $^1\text{O}_2$  quantum yield is considered the main requirement for a good PS [30], but comparison of the photodynamic efficiency of PSs having similar photophysical characteristics revealed that other properties of the PS can also affect PDT efficiency. Among them are the tendency to aggregate, the overall charge and distribution of charges, three-dimensional shape of the molecule, uptake, and subcellular distribution of the PS [15,31–33]. Due to the short half-life and short diffusion distances of  $^1\text{O}_2$  and other photo-generated reactive species in the biological environment, efficiency of photodynamic treatment depends on cytotoxic species that are generated not in the environment but near or inside the biological targets [31,34,35]. This means that, to be photo-efficient, a PS should localize in or very

close to critical biological targets, which points to uptake and subcellular distribution of PSs being key factors directing PDT outcome.

### 2.5. Cellular Uptake of Arene Ruthenium Porphyrin Derivatives

Cellular accumulation of PSs depends mainly on the structure of the compounds. Lipophilicity, number, and position of charges, symmetry, and flexibility of the molecule are among the key features that control uptake and subcellular distribution of PSs [30,32,33]. Figure 5 shows that two of the tetra-substituted derivatives, **Zn-Ru<sub>4a</sub>** and **Ru<sub>4a</sub>**, accumulate to the highest level in cancer cells. The other tetra-substituted compounds, **Zn-Ru<sub>4b</sub>** and **Ru<sub>4b</sub>**, reach intracellular level about half of **Zn-Ru<sub>4a</sub>**. The di-substituted **Zn-Ru<sub>2a</sub>** and **Zn-Ru<sub>2b</sub>** were taken up less efficiently and their cellular concentration did not exceed a quarter of the level of **Zn-Ru<sub>4a</sub>**. The presence of arene ruthenium units at the periphery of the porphyrin plays a role in increasing water solubility, presumably by aquation of the chlorido ligands, thus potentially increasing the internalization of the compound within cancer cells [36]. Cellular uptakes of the di-substituted Zn-free RuPs, **Ru<sub>2a</sub>** and **Ru<sub>2b</sub>**, were the lowest. Such low cellular uptake, combined with low ROS production, can explain the lack of photodynamic activity of these two compounds. Despite equal cellular uptake, **Zn-Ru<sub>4a</sub>** and **Ru<sub>4a</sub>** differed with respect to PDT efficiency, which can be attributed to differences in the production of ROS. Uptake of **Zn-Ru<sub>2a</sub>** and **Zn-Ru<sub>2b</sub>** was relatively low but, at 5  $\mu$ M, both compounds acted as efficient PSs as a consequence of their high ROS-generating capacity, as shown in Figures 3 and 4. In parallel, cellular uptake of the RuPs was measured spectrophotometrically by determining the area under the peak of the Soret band (Figure S3). Due to the low water solubility of the tested compounds, leading to partial aggregation [15], the area under the peaks was very small, which negatively affected the reproducibility of the results. Another important aspect that should be taken into consideration is that most PSs can work by both electron-transfer (Type I) and energy-transfer (Type II) photochemical reactions, and the relative contribution of each of the two mechanisms is strongly affected by the biological environment [31].

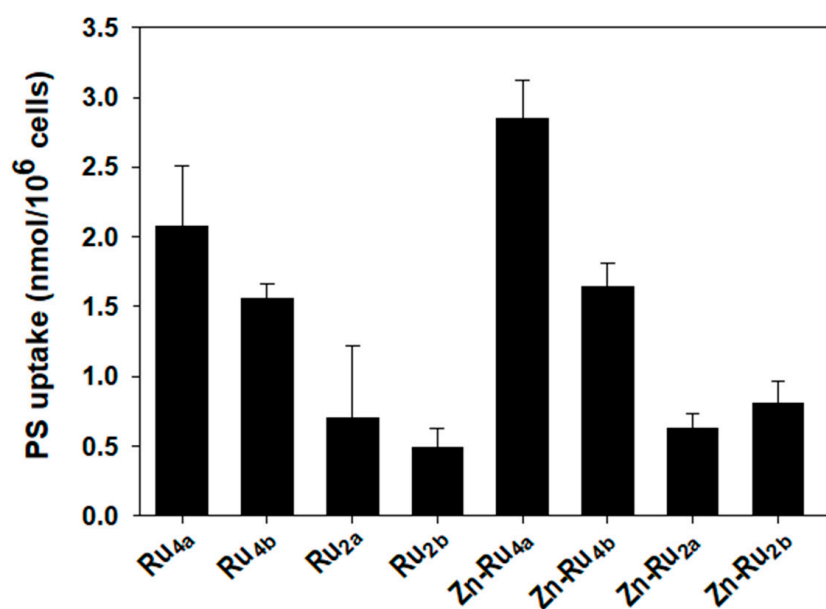


**Figure 5.** Cellular uptake of arene ruthenium porphyrin derivatives. Cells were incubated for 24 h in the dark with 5  $\mu$ M of the compounds. Accumulation of PSs was determined by measuring the area under the fluorescence emission peaks after solubilization of the cells. The concentration of the PS in each sample was determined using a standard curve generated for each individual compound. Data are expressed as mean  $\pm$  S.D. of two independent experiments, each sample was run in duplicate.

## 2.6. Cell Death Mechanisms

Among the factors that determine the type of PDT-induced cell death are the site and the extent of cell damage, which in turn depend on the photo-efficacy, uptake, and subcellular distribution of the PS. Execution of apoptosis requires intact apoptotic machinery, and extensive photo-damage usually leads to necrotic cell death [37].

The compounds investigated in this study differ broadly by ROS yield, cellular uptake, and photo-dynamic efficiency, and it is expected that they might kill cancer cells by different mechanisms. The results presented in Figure 6 and Figure S5 demonstrate that cells illuminated in the presence of Zn-Ru were in a late apoptotic phase. No conclusion about the mechanism of cell death by Zn-free ligands could be drawn due to the low percentage of non-viable cells. The results presented in Figure S6 show a small number of necrotic and apoptotic cells when incubated with the tested compounds in the absence of light.

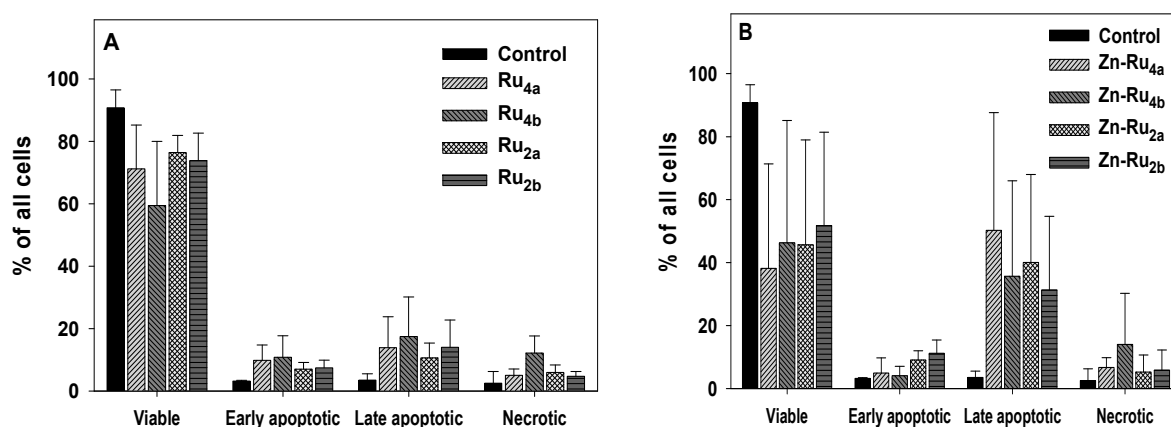


**Figure 6.** Cell death analysis. Cells were preincubated with 5  $\mu$ M arene ruthenium porphyrins for 24 h in the dark. The cells were then illuminated for 30 min, incubated for 4 h, and the mechanism of cell death was determined by flow cytometry using the Annexin V-FITC/7-ADD kit. (A), Zn-free Ru-porphyrins; (B), Zn-Ru derivatives. Data are presented as mean  $\pm$  S.D. of two independent experiments.

As mentioned before, subcellular localization of PSs is among the main factors that control the mechanisms of PDT-induced cell death. In general, PSs that localize in the plasma membrane cause necrotic cell death [37,38]. Since all tested RuPs are lipophilic, it can be expected that they disperse in the lipid bilayer of the plasma membrane. Production of reactive species in such environments initiates free radical chain reactions [33], compromising membrane barrier function and resulting in the leakage of metabolites and ATP [37–39]. Depletion of ATP prevents the activation of apoptotic pathways and leads to necrotic cell death [40]. Another reason for PDT-induced suppression of apoptosis is inactivation of the caspases by photo-generated reactive species [28].

## 3. Materials and Methods

### 3.1. Synthesis

The photosensitizers (PSs) investigated in this study are arene ruthenium porphyrin derivatives, as presented in Figure 1. The complexes are prepared according to published methods [16], following the same strategy: the dinuclear arene ruthenium complexes [Ru(arene)( $\mu$ -Cl)Cl]<sub>2</sub> (arene = *p*-cymene = **a**, arene = phenylpropanol = **b**) react with the pyridyl-containing porphyrin derivatives (5,10,15,20-tetra(4-pyridyl)porphyrin, 5,10,15,20-tetra(4-pyridyl)porphyrin-Zn, 5,15-di(4-pyridyl)-10,20-diphenylporphyrin, and 5,15-di(4-pyridyl)-10,20-diphenylporphyrin-Zn) to give in excellent yield the corresponding di- and tetranuclear complexes (**Ru<sub>2a</sub>**, **Ru<sub>2b</sub>**, **Zn-Ru<sub>2a</sub>**, **Zn-Ru<sub>2b</sub>**, **Ru<sub>4a</sub>**, **Ru<sub>4b</sub>**, **Zn-Ru<sub>4a</sub>**, **Zn-Ru<sub>4b</sub>**). These compounds are soluble in DMSO and slightly soluble in other solvents such as chloroform, water, benzene, ace-tonitrile, dichloromethane, acetone, and ethanol.

### 3.2. Cell Line and Cell Culture

Human colorectal cell line Colo205 was purchased from American Culture Type Collection. Colo205 cells were grown in RPMI-1640 (Gibco BRL, Cergy-Pontoise, France), supplemented with 10% fetal bovine serum (FBS) (Gibco BRL), 100 U/mL penicillin and 100 µg/mL streptomycin (Gibco BRL). Cultures were maintained in a humidified atmosphere with 5% CO<sub>2</sub> at 37 °C.

### 3.3. Light Source

Cell cultures in all experiments were illuminated for 30 min at a fluence of 95 mW/cm<sup>2</sup> (171 J/cm<sup>2</sup>) by an incandescent 300 W broad spectrum lamp (EIKI industrial co. LTD, Osaka, Japan, OHP-3100p). Using such an illumination source avoids the necessity of calculating the irradiation dose for each compound. Spectral characteristics of the light source have been previously published [41]. No change of sample temperature was observed during illumination.

### 3.4. Photo-Production of Reactive Oxygen Species

Reactive oxygen species (ROS) generated by arene ruthenium porphyrin derivatives were measured by the decomposition of DPBF, which was monitored as a decrease in absorbance at 415 nm and is presented as  $\Delta OD_{415nm}/min$ . The reaction mixture contained 3 mL of 9:1 dimethylformamide (DMF):deionized water (ddH<sub>2</sub>O), 50 µM of DPBF prepared in DMSO, and 1 µM of the tested compound. Concentrations of DMF and DMSO at the time of illumination were 90% and 1%, respectively. The mixture was added into a quartz cuvette and was illuminated with visible light at a fluence of 95 mW/cm<sup>2</sup>. Absorbance at 415 nm was measured at 2 min intervals for 10 min. Controls contained all the reaction components except the tested compounds.

### 3.5. Metabolic Activity

Metabolic activity was determined using the 3-(4,5-dimethylthiazol-2-yl)-2,5-diphenyltetrazolium bromide (MTT) assay based on NAD(P)H-dependent enzymatic reduction of MTT to an insoluble, purple-colored formazan [25]. Cells were seeded into a flat-bottom 96-well microplate and incubated overnight to adhere. PSs were added at final concentrations of 1, 2.5, and 5 µM in triplicate wells. The maximal DMSO concentration is 1% in the final concentration and does not cause any significant effect on colon cancer cells [42]. The cells were incubated with PSs in a 5% CO<sub>2</sub> incubator at 37 °C in the dark for 24 h. Control cells were not treated with PSs. After the incubation, the medium was replaced with a medium without phenol red and the plates were illuminated for 30 min at a fluence of 95 mW/cm<sup>2</sup>. After 24 h, 10 µL of MTT reagent prepared by dissolving 5 mg of MTT in 1 mL PBS were added to each well and plates were incubated for 4 h at 37 °C. Formazan crystals were solubilized by adding 200 µL of DMSO per well. Readings were taken at 560 nm (formazan) and 700 nm (background) using a microplate reader [43]. Dark toxicity of the tested PSs was assessed by following the same protocol except that the samples were not illuminated.

### 3.6. Cell Proliferation

The effect of arene ruthenium porphyrin on cell proliferation was investigated by the Sulforhodamine B (SRB) assay. The SRB assay was performed at 0, 24, 48, and 72 h, with zero time remaining immediately after illumination. Cells were fixed with cold TCA to a final concentration of 10%. The plates were then incubated at 4 °C for 1 h and washed five times with deionized water. Cells were stained with 0.4% SRB dissolved in 1% acetic acid, and the wells were washed 5 times with 1% acetic acid to remove unbound stains. The bound dye was solubilized with 10 mM Tris base solution with volume equal to the volume of the original culture medium. The plates were analyzed on a microplate reader at 510 nm and the background was measured at 690 nm [44].

### 3.7. Cellular Uptake of Arene Ruthenium (II) Porphyrins

Cells were seeded in a six-well plate at  $25 \times 10^4$  cells per well. PSs were added at a concentration of 5  $\mu\text{M}$ , and the cells were incubated in the dark for 24 h. The medium was removed and the cells were thoroughly washed with PBS and solubilized with 5% Triton-X. The emission spectra ranging from 500 to 780 nm were determined and cellular accumulation of PSs was assayed by measuring the area under the fluorescence emission peaks after solubilization of the cells, as shown in Figure S1. The number of PSs taken up by the cells was determined using a separate standard curve for each compound.

### 3.8. Cell Death Analysis by Flow Cytometry

For flow cytometry,  $10^6$  cells per well were seeded in a six-well plate and left overnight to adhere. PSs were added at a final concentration of 5  $\mu\text{M}$ , and the cells were incubated in the dark for 24 h. The plates were illuminated for 30 min at a fluence of 95  $\text{mW}/\text{cm}^2$ . After illumination, plates were incubated in the dark for 24 h in a 5%  $\text{CO}_2$  incubator. Mechanisms of cell death were investigated by flow cytometry using the Annexin V-FITC/7-ADD kit according to the manufacturer's instructions (Beckman Coulter Inc., Miami, FA, USA). Each experiment was repeated at least twice with three replicates. One Way Analysis of Variance (ANOVA) was performed using SigmaPlot version 11.0 and  $p$ -value  $\leq 0.05$  was accepted as statistically significant. Results are presented as the mean of at least two independent experiments  $\pm$  S.D.

## 4. Conclusions

In conclusion, the chelation of Zn in the tetrapyrrole ring and increasing the number of arene ruthenium substituents at the periphery increased the photogeneration of ROS, the uptake of the PSs by cancer cells, and the overall photodynamic anticancer efficiency of the tested arene ruthenium porphyrins. Insertion of Zn into the porphyrin rings resulted in a two-fold increase in ROS production compared to the Zn-free analogs. The tetra-substituted Zn-ruthenium porphyrins exhibited superior PDT efficiency compared to the di-substituted derivatives. Similarly, the tetra-substituted Zn-free PSs were more efficient than di-substituted Zn-free analogs. As a result, increasing the number of the arene ruthenium substituents at the periphery of the porphyrin ring augmented the overall photodynamic efficiency of the compounds. Our findings underscore the essential role of arene ruthenium substituents and Zn chelation in enhancing photo-induced ROS production and cellular uptake, two crucial factors for efficient PDT. Additionally, these results motivate further exploration of the potential of these compounds in PDT, including investigations into intracellular localization, photodynamic efficiency in diverse cell lines, and potential applications for in vivo PDT.

**Supplementary Materials:** The following supporting information can be downloaded at <https://www.mdpi.com/article/10.3390/inorganics12030086/s1>. Figure S1. Emission spectra of solubilized cells incubated with arene ruthenium porphyrins at 5  $\mu\text{M}$  determined by spectrofluorometry to determine the cellular uptake of PSs. (A) **Ru**<sub>4a</sub>, (B) **Ru**<sub>4b</sub>, (C) **Ru**<sub>2a</sub>, (D) **Ru**<sub>2b</sub>, (E) **Zn-Ru**<sub>4a</sub>, (F) **Zn-Ru**<sub>4a</sub>, (G) **Zn-Ru**<sub>4b</sub>, (H) **Zn-Ru**<sub>2b</sub>. Figure S2. Toxicity in the dark. Cells were preincubated with 5  $\mu\text{M}$  of PSs for 24 h in the dark and were kept wrapped in aluminum foil for 30 min on the illumination platform. Metabolic activity was determined by the MTT assay and presented as a percentage of MTT reduction to formazan, compared to controls. Mean of three independent experiments  $\pm$  S.D. is shown. Figure S3. Absorbance spectra of solubilized cells incubated with arene ruthenium porphyrins at 5  $\mu\text{M}$ . (A) **Ru**<sub>4a</sub>, (B) **Ru**<sub>4b</sub>, (C) **Ru**<sub>2a</sub>, (D) **Ru**<sub>2b</sub>, (E) **Zn-Ru**<sub>4a</sub>, (F) **Zn-Ru**<sub>4a</sub>, (G) **Zn-Ru**<sub>4b</sub>, (H) **Zn-Ru**<sub>2b</sub>. Figure S4. Effect of arene ruthenium porphyrins on cell proliferation. Cell cultures were preincubated with 5  $\mu\text{M}$  PSs for 24 h, kept in the dark, and SRB assay was then performed. Panel (A), Zn-free Ru-porphyrins; Panel (B), Zn-Ru derivatives. Results are presented as  $\text{OD}_{510\text{ nm}}$  corresponding to the number of adhered viable cells. Data are expressed as mean  $\pm$  S.D. of three independent experiments. Figure S5. Flow cytometry analysis of illuminated cells. Colo205 cells were preincubated with 5  $\mu\text{M}$  of the PSs for 24 h and then illuminated for 30 min. The readings were taken after 24 h. Control (A), **Ru**<sub>4a</sub> (B), **Ru**<sub>4b</sub> (C), **Ru**<sub>2a</sub> (D), **Ru**<sub>2b</sub> (E), **Zn-Ru**<sub>4a</sub> (F), **Zn-Ru**<sub>4b</sub> (G),

**Zn-Ru<sub>2a</sub>** (H), **Zn-Ru<sub>2b</sub>** (I). The lower left quadrant represents viable cells, the lower right quadrant represents early apoptotic cells, the upper right quadrant represents late apoptotic cells, and the upper left quadrant represents necrotic cells. Results of one representative experiment are shown. Figure S6. Flow cytometry profiles of non-illuminated cells. Colo205 cells preincubated with 5  $\mu$ M of the PSs for 24 h and kept in the dark. The readings were taken after 24 h. Control (A), **Ru<sub>4a</sub>** (B), **Ru<sub>4b</sub>** (C), **Ru<sub>2a</sub>** (D), **Ru<sub>2b</sub>** (E), **Zn-Ru<sub>4a</sub>** (F), **Zn-Ru<sub>4b</sub>** (G), **Zn-Ru<sub>2a</sub>** (H), **Zn-Ru<sub>2b</sub>** (I). The lower left quadrant represents viable cells, the lower right quadrant represents early apoptotic cells, the upper right quadrant represents late apoptotic cells, and the upper left quadrant represents dead necrotic cells. Results of one representative experiment are shown. Table S1. UV-vis maximum absorption and molar extinction coefficient [ $\epsilon$  ( $\times 10^{-3} \text{ M}^{-1} \text{ cm}^{-1}$ )] determined in ethanol. Tested compounds were dissolved in DMSO at concentration of 1000  $\mu$ M and stock solutions were diluted in ethanol. Concentrations of 10, 5, 2.5, and 1  $\mu$ M were used for spectral analysis.

**Author Contributions:** Conceptualization, L.B., M.G.-V. and M.D.-A.; software, Z.J. and L.B.; formal analysis, Z.J.; investigation, Z.J.; resources, L.B. and B.T.; writing—original draft preparation, Z.J.; writing—review and editing, B.T., B.L. and L.B.; supervision, L.B. and B.T.; project administration, B.T., B.L. and L.B.; funding acquisition, L.B. All authors have read and agreed to the published version of the manuscript.

**Funding:** This study was funded by Kuwait University grant MB01/18, Kuwait. We are grateful to OMICSRU/RCF, projects SRUL02/13 and GM01/15, Kuwait University, Kuwait.

**Data Availability Statement:** The data presented in this study are openly available in the Open Science Framework (OSF) at <https://osf.io/s9na7>, accessed on 12 December 2023.

**Acknowledgments:** We thank Fatima Sequeira and Simranbir Kaur and all of the people involved in the project; we are grateful to OMICSRU/RCF, projects SRUL02/13 and GM01/15, and we thank the RCF (Research Core Faculty) support staff for the great help.

**Conflicts of Interest:** The authors declare no conflicts of interest.

## References

1. Mármol, I.; Sánchez-de-Diego, C.; Pradilla Dieste, A.; Cerrada, E.; Rodriguez Yoldi, M.J. Colorectal carcinoma: A general overview and future perspectives in colorectal cancer. *Int. J. Mol. Sci.* **2017**, *18*, 197. [[CrossRef](#)] [[PubMed](#)]
2. Simon, K. Colorectal cancer development and advances in screening. *Clin. Interv. Aging* **2016**, *11*, 967–976. [[CrossRef](#)] [[PubMed](#)]
3. Schwartz, R.N.; Blanke, C.D.; Pesko, L.J. Targeted therapies in the treatment of colorectal cancer: What managed care needs to know. *J. Manag. Care Pharm.* **2004**, *10*, S2–S13. [[PubMed](#)]
4. Vicente, M. Porphyrin-based sensitizers in the detection and treatment of cancer: Recent progress. *Curr. Med. Chem. Anticancer Agents* **2001**, *1*, 175–194. [[CrossRef](#)] [[PubMed](#)]
5. Bhattacharya, D.; Mukhopadhyay, M.; Shivam, K.; Tripathy, S.; Patra, R.; Pramanik, A. Recent developments in photodynamic therapy and its application against multidrug resistant cancers. *Biomed. Mater.* **2023**, *18*, 062005. [[CrossRef](#)] [[PubMed](#)]
6. Wilkinson, F.; Helman, W.P.; Ross, A.B. Rate constants for the decay and reactions of the lowest electronically excited singlet state of molecular oxygen in solution. An expanded and revised compilation. *J. Phys. Chem. Ref. Data* **1995**, *24*, 663–677. [[CrossRef](#)]
7. Ishchenko, A.; Syntugina, A. Structure and Photosensitizer Ability of Polymethine Dyes in Photodynamic Therapy: A Review. *Theor. Exp. Chem.* **2023**, *58*, 373–401. [[CrossRef](#)]
8. Redmond, R.W.; Kochevar, I.E. Spatially resolved cellular responses to singlet oxygen. *Photochem. Photobiol.* **2006**, *82*, 1178–1186. [[CrossRef](#)]
9. Ogilby, P.R. Singlet oxygen: There is indeed something new under the sun. *Chem. Soc. Rev.* **2010**, *39*, 3181–3209. [[CrossRef](#)]
10. Kochevar, I.E.; Lynch, M.C.; Zhuang, S.; Lambert, C.R. Singlet Oxygen, but not Oxidizing Radicals, Induces Apoptosis in HL-60 Cells. *Photochem. Photobiol.* **2000**, *72*, 548–553. [[CrossRef](#)]
11. Buytaert, E.; Dewaele, M.; Agostinis, P. Molecular effectors of multiple cell death pathways initiated by photodynamic therapy. *Biochim. Biophys. Acta* **2007**, *1776*, 86–107. [[CrossRef](#)]
12. Kessel, D.; Luo, Y.; Deng, Y.; Chang, C. The role of subcellular localization in initiation of apoptosis by photodynamic therapy. *Photochem. Photobiol.* **1997**, *65*, 422–426. [[CrossRef](#)]
13. Jensen, T.J.; Vicente, M.G.H.; Luguaya, R.; Norton, J.; Fronczek, F.R.; Smith, K.M. Effect of overall charge and charge distribution on cellular uptake, distribution and phototoxicity of cationic porphyrins in HEp2 cells. *J. Photochem. Photobiol. B* **2010**, *100*, 100–111. [[CrossRef](#)]
14. Schaberle, F.A. Assessment of the actual light dose in photodynamic therapy. *Photodiagn. Photodyn. Ther.* **2018**, *23*, 75–77. [[CrossRef](#)] [[PubMed](#)]
15. Benov, L. Photodynamic therapy: Current status and future directions. *Med. Princ. Pract.* **2015**, *24* (Suppl. 1), 14–28. [[CrossRef](#)]

16. Schmitt, F.; Govindaswamy, P.; Süß-Fink, G.; Ang, W.H.; Dyson, P.J.; Juillerat-Jeanneret, L.; Therrien, B. Ruthenium porphyrin compounds for photodynamic therapy of cancer. *J. Med. Chem.* **2008**, *51*, 1811–1816. [[CrossRef](#)] [[PubMed](#)]
17. Gallardo-Villagrán, M.; Paulus, L.; Champavier, Y.; Leger, D.Y.; Therrien, B.; Liagre, B. Combination of tetrapyrrolylporphyrins and arene ruthenium (II) complexes to treat synovial sarcoma by photodynamic therapy. *J. Porphyr. Phthalocyanines* **2022**, *26*, 533–541. [[CrossRef](#)]
18. Lucky, S.S.; Soo, K.C.; Zhang, Y. Nanoparticles in photodynamic therapy. *Chem. Rev.* **2015**, *115*, 1990–2042. [[CrossRef](#)]
19. Jiang, Z.; Shao, J.; Yang, T.; Wang, J.; Jia, L. Pharmaceutical development, composition and quantitative analysis of phthalocyanine as the photosensitizer for cancer photodynamic therapy. *J. Pharm. Biomed. Anal.* **2014**, *87*, 98–104. [[CrossRef](#)]
20. Huang, H.; Yu, B.; Zhang, P.; Huang, J.; Chen, Y.; Gasser, G.; Ji, L.; Chao, H. Highly charged ruthenium (II) polypyridyl complexes as lysosome-localized photosensitizers for two-photon photodynamic therapy. *Angew. Chem. Int. Ed. Engl.* **2015**, *54*, 14049–14052. [[CrossRef](#)]
21. Liang, G.; Wang, L.; Yang, Z.; Koon, H.; Mak, N.; Chang, C.K.; Xu, B. Using enzymatic reactions to enhance the photodynamic therapy effect of porphyrin dityrosine phosphates. *Chem. Commun.* **2006**, *48*, 5021–5023. [[CrossRef](#)] [[PubMed](#)]
22. Kaspler, P.; Lazic, S.; Forward, S.; Arenas, Y.; Mandel, A.; Lilge, L. A ruthenium (II) based photosensitizer and transferrin complexes enhance photo-physical properties, cell uptake, and photodynamic therapy safety and efficacy. *Photochem. Photobiol. Sci.* **2016**, *15*, 481–495. [[CrossRef](#)]
23. Gunaydin, G.; Gedik, M.E.; Ayan, S. Photodynamic therapy—Current limitations and novel approaches. *Front. Chem.* **2021**, *9*, 691697. [[CrossRef](#)]
24. Zamojć, K.; Zdrowowicz, M.; Rudnicki-Velasquez, P.B.; Krzyminiński, K.; Zaborowski, B.; Niedziałkowski, P.; Jacewicz, D.; Chmurzyński, L. The development of 1, 3-diphenylisobenzofuran as a highly selective probe for the detection and quantitative determination of hydrogen peroxide. *Free Radic. Res.* **2017**, *51*, 38–46. [[CrossRef](#)]
25. Germain, N.; Dhayer, M.; Boileau, M.; Fovez, Q.; Kluza, J.; Marchetti, P. Lipid metabolism and resistance to anticancer treatment. *Biology* **2020**, *9*, 474. [[CrossRef](#)] [[PubMed](#)]
26. Broekgaarden, M.; Weijer, R.; van Gulik, T.M.; Hamblin, M.R.; Heger, M. Tumor cell survival pathways activated by photodynamic therapy: A molecular basis for pharmacological inhibition strategies. *Cancer Metastasis Rev.* **2015**, *34*, 643–690. [[CrossRef](#)]
27. Weijer, R.; Clavier, S.; Zaal, E.A.; Pijls, M.M.; van Kooten, R.T.; Vermaas, K.; Leen, R.; Jongejan, A.; Moerland, P.D.; van Kampen, A.H. Multi-OMIC profiling of survival and metabolic signaling networks in cells subjected to photodynamic therapy. *Cell Mol. Life Sci.* **2017**, *74*, 1133–1151. [[CrossRef](#)] [[PubMed](#)]
28. Charara, M.; Tovmasyan, A.; Batinic-Haberle, I.; Craik, J.; Benov, L. Post-illumination cellular effects of photodynamic treatment. *PLoS ONE* **2017**, *12*, e0188535. [[CrossRef](#)]
29. Keibler, M.A.; Wasylenko, T.M.; Kelleher, J.K.; Iliopoulos, O.; Vander Heiden, M.G.; Stephanopoulos, G. Metabolic requirements for cancer cell proliferation. *Cancer Metab.* **2016**, *4*, 16. [[CrossRef](#)]
30. Bacellar, I.O.; Tsubone, T.M.; Pavani, C.; Baptista, M.S. Photodynamic efficiency: From molecular photochemistry to cell death. *Int. J. Mol. Sci.* **2015**, *16*, 20523–20559. [[CrossRef](#)]
31. Oliveira, C.S.; Turchiello, R.; Kowaltowski, A.J.; Indig, G.L.; Baptista, M.S. Major determinants of photoinduced cell death: Subcellular localization versus photosensitization efficiency. *Free Radic. Biol. Med.* **2011**, *51*, 824–833. [[CrossRef](#)]
32. Ezzeddine, R.; Al-Banaw, A.; Tovmasyan, A.; Craik, J.D.; Batinic-Haberle, I.; Benov, L.T. Effect of molecular characteristics on cellular uptake, subcellular localization, and phototoxicity of Zn (II) N-alkylpyridylporphyrins. *J. Biol. Chem.* **2013**, *288*, 36579–36588. [[CrossRef](#)]
33. Odeh, A.M.; Craik, J.D.; Ezzeddine, R.; Tovmasyan, A.; Batinic-Haberle, I.; Benov, L.T. Targeting mitochondria by Zn (II) N-alkylpyridylporphyrins: The impact of compound sub-mitochondrial partition on cell respiration and overall photodynamic efficacy. *PLoS ONE* **2014**, *9*, e108238. [[CrossRef](#)] [[PubMed](#)]
34. Castano, A.P.; Demidova, T.N.; Hamblin, M.R. Mechanisms in photodynamic therapy: Part one—Photosensitizers, photochemistry and cellular localization. *Photodiagn. Photodyn. Ther.* **2004**, *1*, 279–293. [[CrossRef](#)] [[PubMed](#)]
35. Mroz, P.; Huang, Y.-Y.; Janjua, S.; Zhiyentayev, T.; Ruzié, C.; Borbas, K.E.; Fan, D.; Krayner, M.; Balasubramanian, T.; Yang, E.K. In New stable synthetic bacteriochlorins for photodynamic therapy of melanoma. In *Photodynamic Therapy: Back to the Future*; SPIE: Bellingham, WA, USA, 2009. [[CrossRef](#)]
36. Patra, M.; Joshi, T.; Pierroz, V.; Ingram, K.; Kaiser, M.; Ferrari, S.; Spingler, B.; Keiser, J.; Gasser, G. DMSO-Mediated Ligand Dissociation: Renaissance for Biological Activity of N-Heterocyclic-[Ru-( $\eta^6$ -arene)-Cl<sub>2</sub>] Drug Candidates. *Chemistry* **2013**, *19*, 14768–14772. [[CrossRef](#)] [[PubMed](#)]
37. Mroz, P.; Yaroslavsky, A.; Kharkwal, G.B.; Hamblin, M.R. Cell death pathways in photodynamic therapy of cancer. *Cancers* **2011**, *3*, 2516–2539. [[CrossRef](#)]
38. Kessel, D.; Poretz, R. Sites of photodamage induced by photodynamic therapy with a chlorin e6 triacetoxymethyl ester (CAME). *Photochem. Photobiol.* **2000**, *71*, 94–96. [[CrossRef](#)]
39. Al-Mutairi, D.A.; Craik, J.D.; Batinic-Haberle, I.; Benov, L.T. Photosensitizing action of isomeric zinc N-methylpyridylporphyrins in human carcinoma cells. *Free Radic. Res.* **2006**, *40*, 477–483. [[CrossRef](#)]
40. Donohoe, C.; Senge, M.O.; Arnaut, L.G.; Gomes-da-Silva, L.C. Cell death in photodynamic therapy: From oxidative stress to anti-tumor immunity. *Biochim. Biophys. Acta Rev. Cancer* **2019**, *1872*, 188308. [[CrossRef](#)]

41. Thomas, M.; Craik, J.D.; Tovmasyan, A.; Batinic-Haberle, I.; Benov, L.T. Amphiphilic cationic Zn-porphyrins with high photodynamic antimicrobial activity. *Future Microbiol.* **2015**, *10*, 709–724. [[CrossRef](#)]
42. Da Violante, G.; Zerrouk, N.; Richard, I.; Provot, G.; Chaumeil, J.C.; Arnaud, P. Evaluation of the cytotoxicity effect of dimethyl sulfoxide (DMSO) on Caco2/TC7 colon tumor cell cultures. *Biol. Pharm. Bull.* **2002**, *25*, 1600–1603. [[CrossRef](#)] [[PubMed](#)]
43. Berridge, M.V.; Herst, P.M.; Tan, A.S. Tetrazolium dyes as tools in cell biology: New insights into their cellular reduction. *Biotechnol. Annu. Rev.* **2005**, *11*, 127–152. [[CrossRef](#)] [[PubMed](#)]
44. Skehan, P.; Storeng, R.; Scudiero, D.; Monks, A.; McMahon, J.; Vistica, D.; Warren, J.T.; Bokesch, H.; Kenney, S.; Boyd, M.R. New colorimetric cytotoxicity assay for anticancer-drug screening. *J. Natl. Cancer Inst.* **1990**, *82*, 1107–1112. [[CrossRef](#)] [[PubMed](#)]

**Disclaimer/Publisher’s Note:** The statements, opinions and data contained in all publications are solely those of the individual author(s) and contributor(s) and not of MDPI and/or the editor(s). MDPI and/or the editor(s) disclaim responsibility for any injury to people or property resulting from any ideas, methods, instructions or products referred to in the content.